Journal of Propulsion and Power
Vol. 32, No. 2, March-April 2016

Generation of Vortex Lift Through Reduction of Rotor/Stator Gap in Turbomachinery

Lin Du* and Xiaofeng Sun†
Beijing University of Aeronautics and Astronautics, 100191 Beijing, People's Republic of China
and
Vigor Yang‡
Georgia Institute of Technology, Atlanta, Georgia 30332

DOI: 10.2514/1.B35858

The axial gap between blade rows in turbomachinery should be minimized in order to reduce size requirements and increase efficiency; although, there is a tradeoff between gap width and flow steadiness. The aerodynamic interaction between rotors and stators influences system performance under both steady and transient conditions. To investigate the basic physical mechanisms associated with the rotor/stator interaction, an efficient numerical scheme for solving unsteady, viscous flows on a quasi-three-dimensional coordinate system is established using an immersed boundary method. The data transfer between moving and stationary grids that slip against each other in traditional numerical methods is avoided. The effects of the axial gap between adjacent blade rows are studied by considering the flow evolution through a rotor and stator stage in different Reynolds number regimes. Results indicate that reduced blade gap leads to high lift on the rotor blade and improved stage loading. At the same time, the rotor/stator interaction increases flow unsteadiness, which may in turn increase noise and vibration. It is found that the reduced blade gap does not always improve performance, in spite of the generation of vortex lift. The present work provides guidelines for optimization of the axial gap between blade rows for turbomachinery design.

Nomenclature

C_d	=	drag coefficient
C_l	=	lift coefficient
C_p	=	static pressure coefficient
C_s	=	width of stream surface
c	=	chord
d	=	diameter of cylinder
e	=	internal energy
F_x, F_y	=	boundary forces
$\boldsymbol{f}$	=	boundary force density
h	=	enthalpy
L_x	=	length in x coordinates of computational zone
Ma	=	Mach number
m, θ	=	coordinates of stream surface
p^*	=	total pressure
Re	=	Reynolds number
St	=	Strouhal number
U	=	velocity of incoming flow at inlet
U_∞	=	freestream velocity
V	=	moving velocity of rotor blade
$\boldsymbol{v}$	=	fluid velocity
α_1, α_2	=	stagger angle
Γ_1	=	circulation around rotor
Γ_2	=	circulation of shedding vortex
δ	=	axial gap
μ	=	dynamic viscosity
ρ	=	density
$\hat{\tau}_{ij}$	=	viscous stress tensor
ϕ	=	U/V, flow coefficient
ψ	=	time-averaged total-to-total pressure rise coefficient
ψ_t	=	instantaneous total-to-total pressure rise coefficient

Received 22 April 2015; revision received 17 September 2015; accepted for publication 19 September 2015; published online 22 December 2015.

*Postdoc Research Fellow, School of Jet Propulsion; lindu_buaa@sina.cn.
†Professor, School of Jet Propulsion; sunxf@buaa.edu.cn (Corresponding Author).
‡William R. T. Oakes Professor and Chair, School of Aerospace Engineering; vigor.yang@aerospace.gatech.edu.

I. Introduction

A COMPACT turbomachinery design can be achieved by reducing the axial gap between blade rows. This practice, however, has a strong effect on the flow development, and it must be treated with care. Experiments in turbomachinery have proved that unsteady interactions between blade rows, including potential-flow and wake interaction, have a significant influence on stage performance, loading, noise, and response to impressed disturbances. Because unsteadiness in the flowfield leads to enhanced system response and noise, blade rows must be kept at a certain distance from each other to minimize rotor/stator interaction.

Several studies [1–4] have suggested, based on both computational and experimental results, that flow unsteadiness can be reduced as the axial gap between adjacent rows is increased. Smith [5] observed, however, in a series of experiments on a four-stage low-speed compressor, that the average total pressure efficiency increases if the axial gap between rotors and stators is reduced. This phenomenon has also been observed in recent investigations [6–9]. The process can be modeled using the theory proposed by Smith [10], based on wake recovery, which has a significant impact on the efficiency of a turbomachine. Most of the existing studies [5–9], however, focus on wake decay (which is dominated by wake stretching [11]) and entropy generation. It is thought that the stage loss caused by wake mixing can be suppressed by the interaction between the wake and the blade row when the axial gap is reduced. In practice, determination of an optimal axial gap remains a problem of concern, given the significant benefits of understanding and designing for reduced size and increased efficiency.

In addition to stage efficiency, stage loading is another important turbomachinery performance indicator. Furber and Ffowcs Williams [12] reported that the stage loading of an axial pump could be improved by reducing the axial gap between blade rows. A higher stage rise of total pressure was observed with a smaller axial dimension of the pump in experiment. Furber and Ffowcs Williams attributed the improvement to the Weis–Fogh [13,14] mechanism. A critical factor of this mechanism, the effect of unsteady vortex, however, was not taken into account in their steady potential-flow model, and rotor loading, which is determined at the instant of blade contact, was assumed to be constant. The Weis–Fogh mechanism [13,14] was discovered in the "clap-and-fling" motion of a small *Encarsia formosa* by Weis–Fogh [13]. Another kind of interaction is the forewing and hindwing interaction seen in dragonfly flight, indicated by the variations of the phase relation between them during different maneuvers [15–23]. Sun and Lan [15] investigated the lift requirements for a hovering dragonfly using a three-dimensional (3-D) Navier–Stokes solver with overset grid method. It was found that the interaction effect between the two wings reduced the vertical forces on the fore- and hindwings. This effect was also observed in the study by Wang and Sun [16]. Wang and Russell [21] concluded that the aerodynamic power expended was reduced when the wings moved out of phase, and the force was enhanced when the wings moved in phase. Zhang and Lu [22] found that the interaction between the fore- and hindwings effectively enhanced the lift force and reduced the drag force on the wings compared to two independent wings. In the dragonfly flight, the anomalously high-lift coefficients (two to six) were observed, which were difficult to explain using quasi-steady analysis [18–20]. The fore- and hindwings were about a wing's width apart, which was close enough for them to interact hydrodynamically [21].

Li and Lu [24] investigated the dynamics of a flapping plate using a viscous vortex-ring model. It was found that the force and power of the flapping plate were dominated by the vortical structures near the body. The impulse of each vortical structure was close to the momentum of the plate transferred to the flow for the formation of such a vortical structure. For a small axial gap, the unsteady interaction between a rotor and a stator was enhanced, and vortex shedding undoubtedly played a very important role in determining the aerodynamic performance of a stage. The motivation of the present work is to investigate the effect of shedding vortices, which was not included in the inviscid model of Furber and Ffowcs Williams [12], when the axial gap between blade rows is reduced. It is expected that high unsteady lift coefficients can be generated by reducing axial gap to enhance rotor/stator interaction.

In earlier studies on the Weis–Fogh mechanism [12,14–27], the high unsteady lift generated on the wing/blade was thought to be related to the circulation around the wing/blade surfaces. Maxworthy [25], however, indicated that the sign of the circulation around the wing surface was actually opposite to that in the shedding vortex. The loading of a rotor blade was determined by the inflow U_∞ and the circulation around the blade, as shown in Fig. 1. On the basis of Kelvin's theorem, the circulation Γ_1 was influenced by the intensity of the shedding vortex Γ_2. Thus, for a given inflow U_∞, if the circulation Γ_1 was enhanced by shedding vortices generated by the rotor/stator interaction when the axial gap was reduced, the rotor blade force and stage loading could be increased accordingly. Kelvin's circulation theorem has long been employed to provide a qualitative understanding of this phenomenon. Quantitative analysis, however, is yet to be performed. The present numerical work deals quantitatively with the evolution of distributions of pressure, velocity, and vorticity during the rotor/stator interaction. The study conducted by Li and Lu [24] showed that the force and power generated by a flapping wing were closely linked to the local vortical structures. In the present study, the relationship between stage loading and shedding vortices is investigated by means of comprehensive simulations of the flow evolution of a compressor stage. A new approach is developed to increase stage loading through the vortex lift generated by the rotor/stator interaction. Unsteady flow characteristics are also discussed in an effort to determine an optimal axial gap.

For most existing numerical analyses of turbomachinery flows, conventional structured- or unstructured-grid approaches are used to discretize the governing equations on a curvilinear grid that conforms

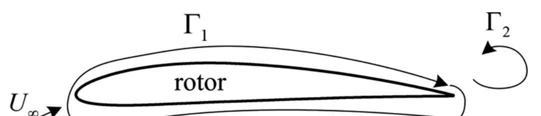

Fig. 1 Circulation around rotor and shedding vortex.

to the boundaries of blades. Considering the relative motion between blades, the computational domain must be subdivided into zones, and the grid for each zone is generated independently. The treatment of the zonal boundary conditions thus has a significant impact on the accuracy and stability of the calculation. Patched and overlaid grids are generally used to interpolate the data at the zonal boundaries, as in the works of Rai [28,29], Giles [30], Chima [31], and Jorgenson and Chima [32]. Rai stressed the importance of conservative treatment of the zonal boundaries [28,29]. When the axial gap between blade rows is reduced, two difficulties arise in simulations using conventional numerical schemes. First, orthogonality is difficult to satisfy near the blade and zonal boundaries as the blade rows approach each other. Second, high gradients of velocity, pressure, and density appear, due to the rotor/stator interactions caused by a smaller axial gap. Interpolation errors thus occur between different computational zones, and it becomes more difficult to obtain accurate results.

The rotor/stator interaction involves moving boundaries. In recent decades, volume-of-fluid [33], level-set [34], vortex [35–37], and immersed-boundary (IB) [38,39] methods have been developed for various types of moving-boundary problems. Because the IB method is easily combined with Chima's [31] and Jorgenson and Chima's model [32], in which circumferential flow could be directly included in a cylindrical grid, this method is chosen in the present work. Based on the IB method, the unsteady flow passing multiple moving bodies can be solved on fixed simple orthogonal meshes. To avoid data exchange at the interface between blade rows, a numerical scheme is established to simulate the unsteady flow associated with the rotor/stator interaction. The present method has been employed for treating fluid–structure interactions by Zhong and Sun [40], Du et al. [41], and Du and Sun [42]. Several complicated nonlinear coupling and flow transition phenomena were captured. The method was also used to simulate the compressible turbulent flow of a modulated fan with pitching blades [43]. Low-frequency sound was generated with high intensity, and the results agreed well with measurements reported by Park and Garcés [44]. Using the present method, the same meshes can be used for different axial gaps and blade shapes; this is beneficial to the investigation of the effects of the axial gap. The generation and evolution of the shedding vortices between blade rows are studied to analyze rotor/stator interactions with a small axial gap.

The present paper is structured as follows. In Sec. II, the numerical scheme is introduced and validated. Its accuracy and stability are demonstrated by simulating two canonical flows. In Sec. III, the computational model for rotor/stator interaction on a stream surface is established following Chima's [31] and Jorgenson and Chima's work [32]. Section IV treats a rotor/stator system for both laminar (incompressible) and turbulent (compressible) flows. Results indicate that the intensity of shedding vortices is intimately influenced by the rotor/stator interaction. A reduced blade gap leads to high lift on the rotor blade and improved stage loading. At the same time, the rotor/stator interaction increases flow unsteadiness, which may in turn increase noise and vibration. It is found that a reduced blade gap does not always improve performance, in spite of the generation of vortex lift. The present work provides guidelines for optimization of the axial gap between blade rows for turbomachinery design. The approach can be conveniently extended to multistage problems.

II. Numerical Scheme and Validation

A. Governing Equations and Construction of Boundary Force

The nondimensional conservation equations for viscous, incompressible flows in two dimensions are

$$\frac{\partial \boldsymbol{v}}{\partial t} + \nabla \cdot (\boldsymbol{v}\boldsymbol{v}) = -\nabla p + \frac{1}{Re}\Delta \boldsymbol{v} + \sum_{k=1}^{M} \boldsymbol{F}_k \tag{1}$$

$$\nabla \cdot \boldsymbol{v} = 0 \tag{2}$$

where $\boldsymbol{v} = (u, v)$ is the velocity, p is the pressure, and Re is the Reynolds number. As illustrated in Fig. 2, the surface Γ is composed of

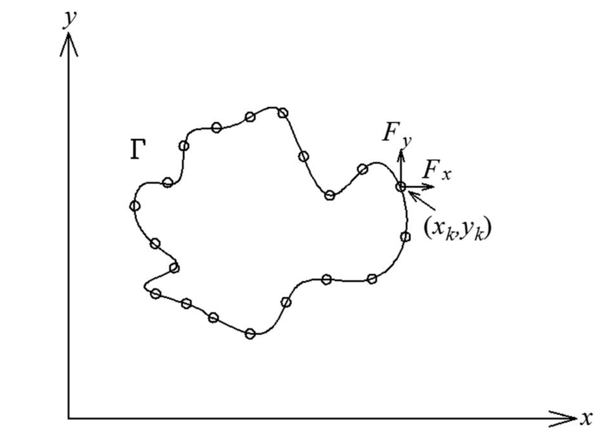

Fig. 2 Sketch of boundary and singular force.

M segments, and $\boldsymbol{F}_k = (F_x, F_y)$ denotes the boundary force from the kth segment of the object surface. The singular force can be given by

$$\boldsymbol{F}_k(x, y, t) = \int_\Gamma \boldsymbol{f}(x_k, y_k, t)\delta(x - x_k)\delta(y - y_k)\,\mathrm{d}s \tag{3}$$

where $\boldsymbol{f}(x_k, y_k, t)$ represents the nondimensional force density. These forces have been constructed in a number of ways, generally based on the immersed boundary method. In the present study, following the model of Goldstein et al. [39], the virtual boundary method is applied to determine the force as

$$\begin{aligned}\boldsymbol{f}(x_k, y_k, t) = {} & \alpha \int_0^t [\boldsymbol{v}_f(x_k, y_k, t') - v_o(x_k, y_k, t')]\,\mathrm{d}t' \\ & + \beta[\boldsymbol{v}_f(x_k, y_k, t) - \boldsymbol{v}_o(x_k, y_k, t)]\end{aligned} \tag{4}$$

where $\boldsymbol{v}_f$ and $\boldsymbol{v}_o$ are the simulated and prescribed velocities of the boundary segment. When α and β are chosen properly, $|\boldsymbol{v}_f(x_k, y_k, t) - \boldsymbol{v}_o(x_k, y_k, t)|$ will stay close to zero and the no-slip flow boundary condition is satisfied. The method proposed by Lai and Peskin [45] is applied in the present numerical scheme to improve the accuracy of boundary conditions.

B. Numerical Discretization

Fluid–structure interactions can be appropriately treated using the immersed boundary method because the entire velocity and pressure fields are obtained by solving the governing equations on fixed rectangular Cartesian meshes. The computational cost of grid regeneration is avoided. The fractional-step method proposed by Armfied and Street [46] for the incompressible Navier–Stokes equations is applied. In the present study, the discretized velocity and pressure fields are staggered, as shown in Fig. 3. Then, Eqs. (1) and (2) are solved as follows:

$$\begin{aligned}\left(\frac{u^* - u^n}{\Delta t}\right)_{I,j} = {} & -\left[\frac{(u^n_{i+1,j})^2 - (u^n_{i,j})^2}{\Delta x} + \frac{u^n_{I,J}v^n_{I,J} - u^n_{I,J-1}v^n_{I,J-1}}{\Delta y}\right] \\ & - \frac{p^n_{i+1,j} - p^n_{i+1,j}}{\Delta x} \\ & + \frac{1}{Re}\left(\frac{u^n_{I+1,j} + 2u^n_{I,j} + u^n_{I-1,j}}{\Delta x^2} + \frac{u^n_{I,j+1} - 2u^n_{I,j} + u^n_{I,j-1}}{\Delta y^2}\right)\end{aligned} \tag{5}$$

$$\begin{aligned}\left(\frac{v^* - v^n}{\Delta t}\right)_{i,J} = {} & -\left[\frac{u^n_{I,J}v^n_{I,J} - u^n_{I-1,J}v^n_{I-1,J}}{\Delta_x} + \frac{(v^n_{i,j+1})^2 - (v^n_{i,j})^2}{\Delta y}\right] \\ & - \frac{p^n_{i,j+1} - p^n_{i,j}}{\Delta y} \\ & + \frac{1}{Re}\left(\frac{v^n_{i+1,J} - 2v^n_{i,J} + v^n_{i-1,j}}{\Delta x^2} + \frac{v^n_{i,J-1} - 2v^n_{i,J} + v^n_{i,J-1}}{\Delta y^2}\right)\end{aligned} \tag{6}$$

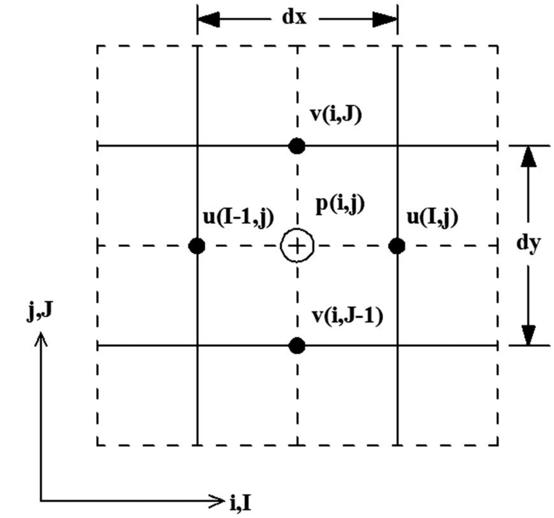

Fig. 3 Variable definition and discretized grid on staggered Cartesian mesh.

$$L\pi = \frac{1}{\Delta t}\left(\frac{u^*_{I,j} - u^*_{I-1,j}}{\Delta x} + \frac{v^*_{i,J} - v^*_{i,J-1}}{\Delta y}\right) \tag{7}$$

$$u^{n+1}_{I,j} = u^n_{I,j} - \Delta t \frac{\pi_{i+1,j} - \pi_{i,j}}{\Delta x} \tag{8}$$

$$v^{n+1}_{i,J} = v^*_{i,J} - \Delta t \frac{\pi_{i,j+1} - \pi_{i,j}}{\Delta y} \tag{9}$$

$$p^{n+1}_{i,j} = p^*_{i,j} + \pi_{i,j} \tag{10}$$

where L is the discrete Laplace operator. The discrete Poisson equation [Eq. (7)] is solved by means of the fast Fourier transformation, which has a cost of the order $\mathcal{O}(N\,\ell_n(N))$, where N is the number of nodes in the grid.

C. Validations of Numerical Method

Two canonical examples are employed to demonstrate the numerical accuracy and robustness of the present scheme. The first is concerned with stationary boundaries, and the second is concerned with moving boundaries.

1. Flow Passing a Stationary Cylinder

A rectangular domain, as shown in Fig. 4, is used to simulate the flow over a stationary cylinder. Spatial resolution is achieved with a grid of $N_x \times N_y = 512 \times 512$. The Reynolds number Re of this flow is defined as

$$Re = \rho U_\infty d/\mu \tag{11}$$

where d is the diameter of the cylinder, μ is the viscosity coefficient, ρ is the density, and U_∞ is the freestream velocity. Simulations are performed in the Reynolds number range of 10,300. The far-field boundary conditions are as follows:

Boundary W:

$$u = 1, \qquad v = 0$$

Boundary E:

$$\frac{\partial u}{\partial x} = 0, \qquad \frac{\partial v}{\partial x} = 0$$

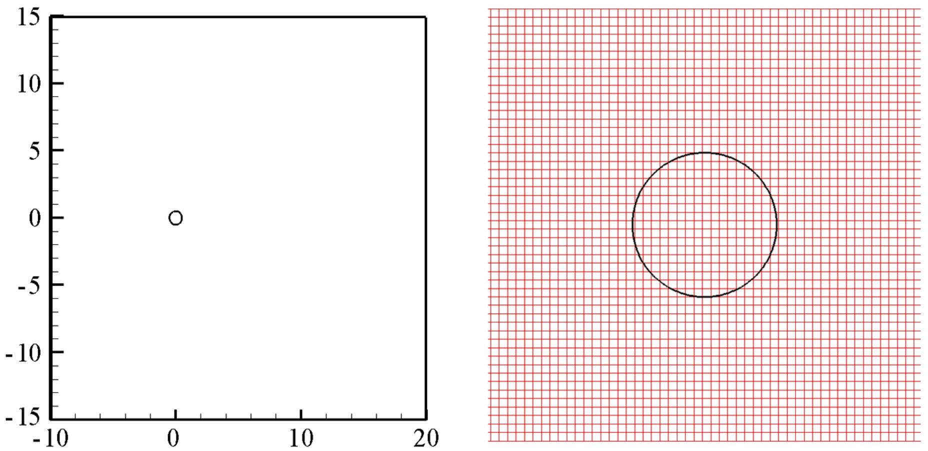

Fig. 4 Computational domain and grid for flow passing a stationary cylinder.

Boundary N:

$$\frac{\partial u}{\partial y} = 0, \qquad v = 0$$

Boundary S:

$$\frac{\partial u}{\partial y} = 0, \qquad v = 0$$

The dimensionless time step is chosen to be 1.5×10^{-3} for all the Reynolds numbers of concern. At each time step, drag and lift can be obtained from

$$F_d(x, y, t) = -\int_{\Gamma} f_x(x_k, y_k, t)\delta(x - x_k)\delta(y - y_k)\,\mathrm{d}s \qquad (12)$$

$$F_l(x, y, t) = -\int_{\Gamma} f_y(x_k, y_k, t)\delta(x - x_k)\delta(y - y_k)\,\mathrm{d}s \qquad (13)$$

The drag and lift coefficients are defined as

$$C_d = \frac{F_d}{\rho U_\infty^2 d/2} \qquad (14)$$

$$C_l = \frac{F_l}{\rho U_\infty^2 d/2} \qquad (15)$$

Figure 5 shows that the calculated time-mean drag coefficients at different Reynolds numbers compare very well with the numerical results of Lima E Silva et al. [47] and the experimental data of Wieselsberger [48]. Figure 6 shows the time histories of the instantaneous drag and lift coefficients for $Re = 200$. The corresponding Strouhal number St is 0.198. The present work gives consistent agreement with previous numerical and experimental results for the flow passing a stationary cylinder.

2. Flow Around a Flapping Wing

This example is concerned with a moving-boundary problem associated with the flow around a hovering wing. The translational and angular velocities of the wing are identical to those described by Miller and Peskin in [49]. A single elliptical wing with an aspect ratio of 10 is considered. One stroke cycle lasts $t_{\mathrm{final}} = 10.8$.

The translational velocity during downstroke is

$$v(t) = 0.5\left[1 + \cos\left(\pi + \frac{\pi t}{0.65}\right)\right], \qquad 0 \le t < 0.65 \qquad (16a)$$

$$v(t) = 1, \qquad 0.65 \le t < 4.75 \qquad (16b)$$

$$v(t) = 0.5\left[1 + \cos\left(\pi \frac{t - 4.75}{0.65}\right)\right], \qquad 4.75 \le t < 5.4 \qquad (16c)$$

where t is the dimensionless time. The sign of the translational velocity during upstroke is opposite that of the downstroke. The angular velocity is given by

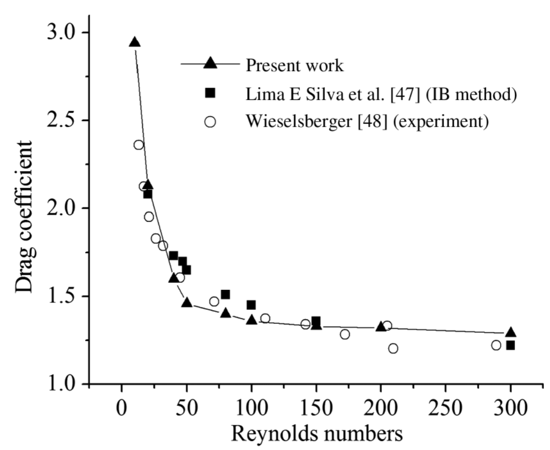

Fig. 5 Time-mean drag coefficients as function of Reynolds number.

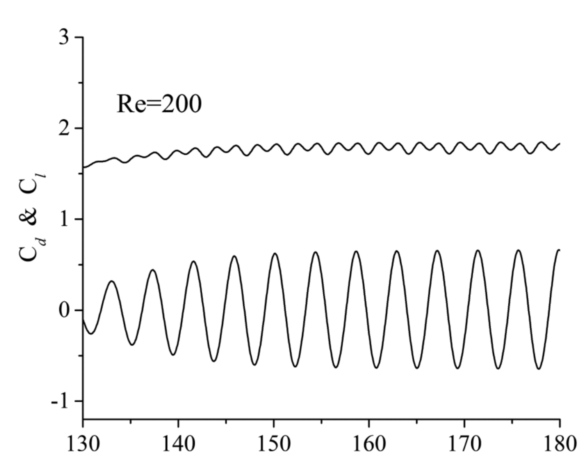

Fig. 6 Temporal evolution of drag and lift coefficients for flow passing stationary cylinder at $Re = 200$.

$$\dot{\theta} = 0, \qquad 0 \le t < 3 \tag{17a}$$

$$\dot{\theta} = 0.5\theta_{\mathrm{rot}}\left[1 - \cos\left(2\pi \frac{t-3}{3.48}\right)\right], \qquad 3 \le t < 6.48 \tag{17b}$$

$$\dot{\theta} = 0, \qquad 6.48 \le T < 10.8 \tag{17c}$$

where $\theta_{\mathrm{rot}} = 0.903$, and the center of rotation is located at 0.2 chord lengths from the leading edge of the wing. The chord length of the elliptical wing is unity. The simulation is carried out using a grid of $N_x \times N_y = 768 \times 512$ and a time step of $\Delta t = 4 \times 10^{-4}$, respectively. Figure 7 shows the vorticity fields around the hovering wing for $Re = 32$ at dimensionless times of $t = 4$ and 10. Figure 8 shows the calculated drag and lift coefficients over one stroke of the flapping wing for $Re = 16$ and 32. Good agreement is achieved with the results reported by Miller and Peskin [49].

III. Computational Model of Rotor/Stator Interaction on a Stream Surface

Chima [31], and Jorgenson and Chima [32] developed a model for analyzing quasi-three-dimensional unsteady viscous flow in turbomachinery. Flow in an axisymmetric stream surface, as shown in Fig. 9, can be effectively solved, where m and θ are coordinates of the stream surface. The radius and thickness of the stream surface are denoted by $r(m)$ and $h(m)$, respectively, and are generally considered to be known functions of m. In the present study, they are assumed to be constants, for the sake of model brevity and clarity. The incompressible Navier–Stokes equations then can be given as:

$$\left(\frac{\partial u_m r}{\partial m} + \frac{\partial u_\theta}{\partial \theta}\right) = 0 \tag{18}$$

$$\rho\frac{\partial u_m r}{\partial t} + \rho\frac{\partial u_m^2 r}{\partial m} + \rho\frac{\partial u_\theta u_m}{\partial \theta} = \frac{\partial pr}{\partial m} + F_m r + \left(\frac{\partial r\sigma_{11}}{\partial m} + \frac{\partial \sigma_{12}}{\partial \theta}\right) \tag{19}$$

$$p\frac{\partial u_\theta r}{\partial t} + \rho\frac{\partial u_\theta u_m r}{\partial m} + \rho\frac{\partial u_\theta^2}{\partial \theta} = -\frac{\partial p}{\partial \theta} + F_\theta r + \left(\frac{\partial r\sigma_{12}}{\partial m} + \frac{\partial \sigma_{22}}{\partial \theta}\right) \tag{20}$$

where

$$\sigma_{11} = \frac{2\mu\partial u_m}{\partial m}, \qquad \sigma_{12} = \mu\left(\frac{\partial u_m}{r\partial\theta} + \frac{\partial u_\theta}{\partial m}\right), \qquad \sigma_{22} = \frac{\partial 2\mu u_\theta}{r\partial\theta} \tag{21}$$

Letting $x = m$, $r\theta = y$, Eqs. (18–21) can be simplified to the same form as the unsteady two-dimensional Navier–Stokes equations, except that the boundary condition in the y direction is periodic.

Rai [28,29], Chima [31], and Jorgenson and Chima [32] applied their model to unsteady rotor/stator interactions. Because multiple grids are employed and the relative motion between the absolute and relative frames of reference is included, the overlapping boundary condition across the interface between the rotor and stator must be

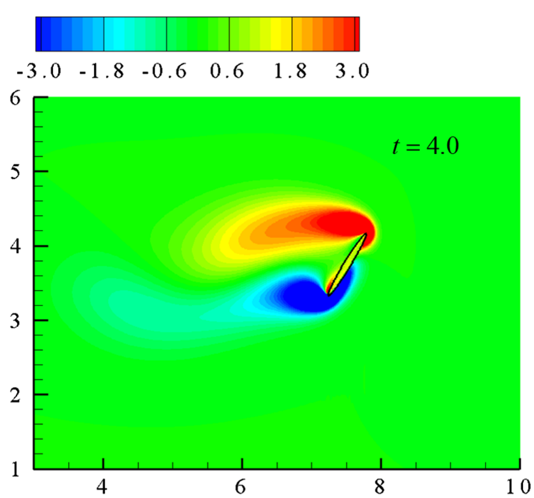

a) t=4

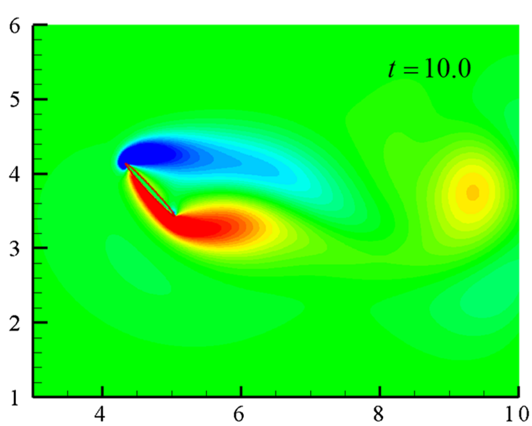

b) t=10

Fig. 7 Vorticity fields of hovering wing at dimensionless times $t = 4$ and $10 (Re = 32)$.

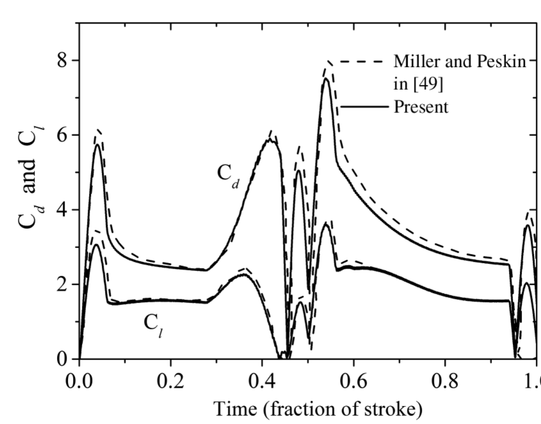

a) Re=16

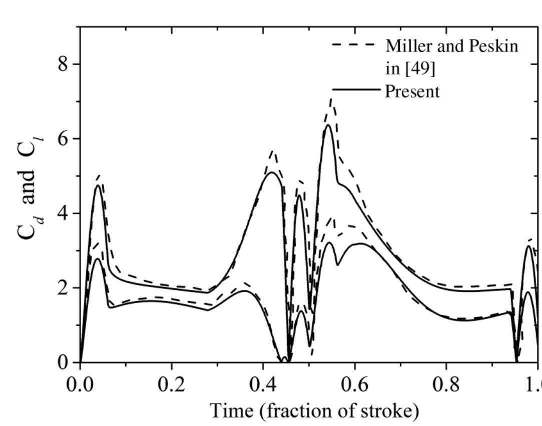

b) Re=32

Fig. 8 Drag and lift coefficients over one stroke of a hovering wing: a) $Re = 16$; and b) $Re = 32$.

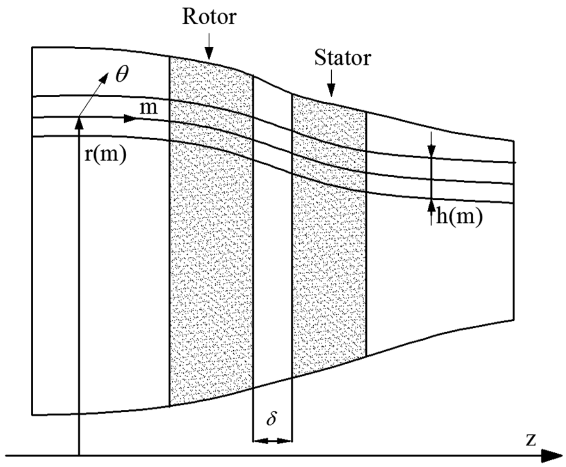

Fig. 9 Quasi-three-dimensional stream surface for compressor rotor/stator stage.

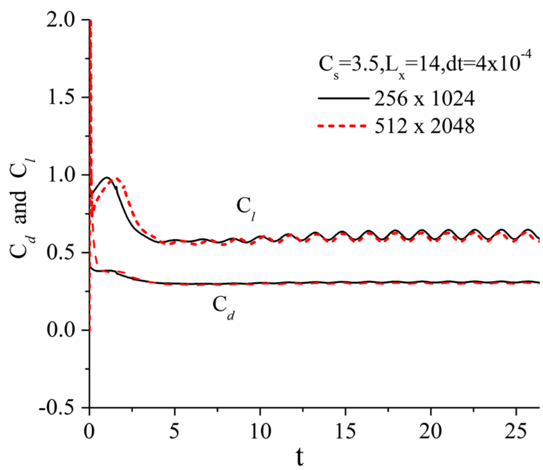

Fig. 10 Temporal evolution of drag and lift coefficients for flow on the stream surface of a stationary blade with different spatial resolutions: $Re = 500$.

treated. In the present model, the IB method is used to allow for use of a single fixed rectangular Cartesian mesh to simulate the flowfield throughout the rotor/stator rows. The transfer of aerodynamic information between computational zones is thus avoided.

IV. Effect of Axial Gap Between Blade Rows and Generation of Vortex Lift

A. Rotor/Stator Interaction in Incompressible Laminar Flow

Most of the previous research [13,49] on vortex lift mechanisms has focused on hovering motion in the low-Reynolds-number regime.

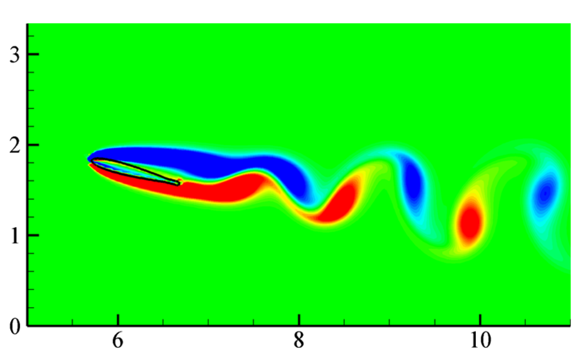

Fig. 11 Vorticity field over stationary blade on a stream surface with spatial resolution of one: $N_x \times N_y = 1024 \times 256$, $L_x = 14$, and $Re = 500$.

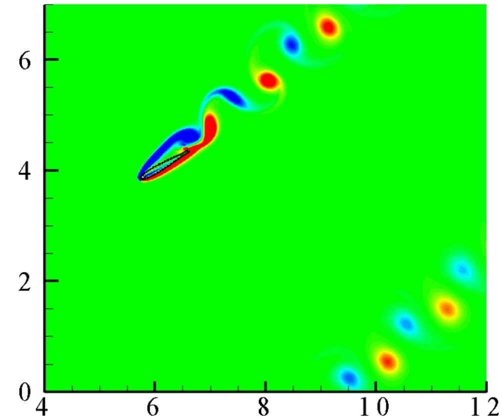

Fig. 12 Vorticity field around moving blade on a stream surface of $Re = 500$ with time step $\Delta t = 4 \times 10^{-4}$.

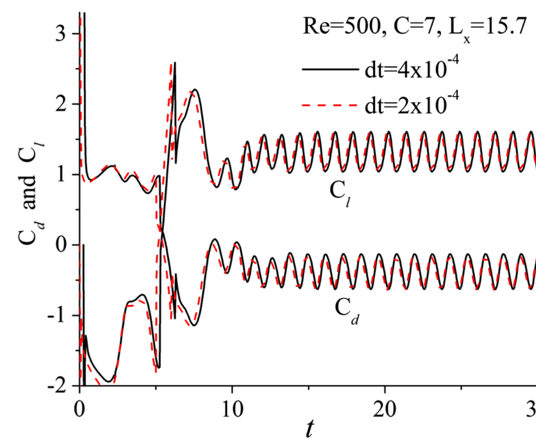

Fig. 13 Time histories of drag and lift coefficients over moving blade on stream surface.

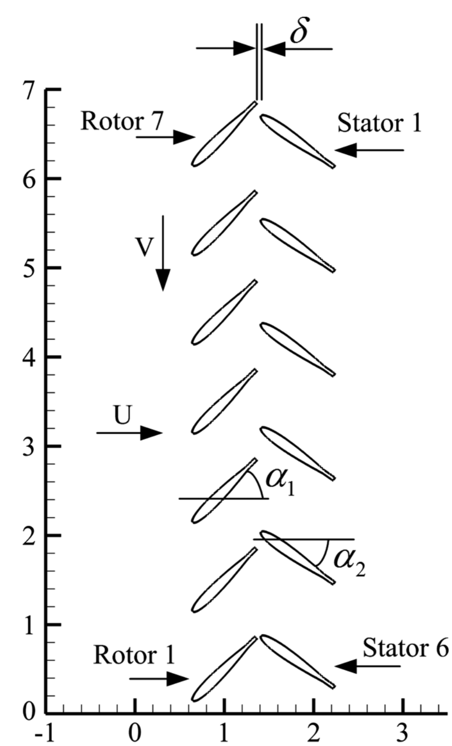

Fig. 14 Single rotor/stator stage, NACA 0012 blade: $\alpha_1 = 45$ deg, $\alpha_1 = -35$ deg, and $\delta/c = 0.03$.

Table 1 Geometric parameters for the laminar flow case

Parameter	Value
c	1
δ/c	0.03, 0.08, 0.13
α_1	45 deg
α_2	−30 deg
V	−1
U	0.3–0.6

We first consider an incompressible, laminar flow at $Re = 500$. Equations (18–20) are solved to simulate the flow on a stream surface with the assumption of constant $r(m)$ and $h(m)$. We first test the numerical convergence for the flow over a NACA0012 airfoil on a stream surface.

The flow evolution over a stationary airfoil is tested at two levels of spatial resolution:

Level 1:

$$N_x \times N_y = 1024 \times 256, \qquad L_x = 14$$

Level 2:

$$N_x \times N_y = 2048 \times 512, \qquad L_x = 14$$

where L_x is defined as the axial length of the computational zone. The width of the stream surface is $C_s = 3.5$. The inlet flow is set to $u = 1$ and $Re = 500$. The stagger angle is -15 deg. A time step of $\Delta t = 4 \times 10^{-4}$ is used for the calculation. Figure 10 shows the calculated instantaneous drag and lift coefficients. The two different levels of spatial resolution lead to almost identical results. Figure 11 shows the calculated vorticity field. Detailed flow evolution is clearly observed, demonstrating the adequacy of the spatial resolution.

In the IB method, temporal convergence of numerical solutions is strongly determined by the boundary movement. The situation over a moving blade is thus studied to verify the time-step independence at $Re = 500$. The grid size is $N_x \times N_y = 1152 \times 512$. The computational domain is $C_s = 7$, $L_x = 15.75$, the inlet flow velocity is $u = 1$, and the moving velocity of the blade is $v = -1$. The stagger angle of the blade is $\alpha = 30$ deg. Time steps of $\Delta t = 4 \times 10^{-4}$ and 2×10^{-4} are used. Figure 12 shows the vorticity fields around the moving blade with a time step of $\Delta t = 4 \times 10^{-4}$. Figure 13 shows that the calculated instantaneous drag and lift coefficients from the two different time steps are in excellent agreement. The time step $\Delta t = 4 \times 10^{-4}$ is therefore used for the simulation of rotor/stator interactions at $Re = 500$.

The third test case involves a stage composed of seven rotor blades (standard NACA0012) and six stator blades, as shown schematically in Fig. 14. The blade rows are designated from rotors 1 to 7 and stators 1 to 6, respectively. The width of the stream surface is $C_s = 7$. Table 1 lists the geometric parameters, where c is the blade chord, V is the moving velocity of rotor blade, δ is the axial gap between blade rows, and U is the inflow velocity. The time t is normalized by the chord and V. The Reynolds number is defined with respect to the rotational velocity of the rotor blade:

$$Re = \rho|V|c/\mu \tag{22}$$

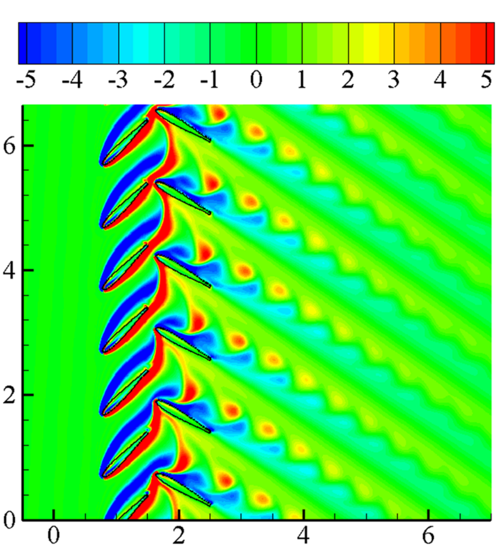

Fig. 15 Vorticity field around stage on stream surface: $Re = 500$, $\delta/c = 0.13$, and $U/V = 0.5$.

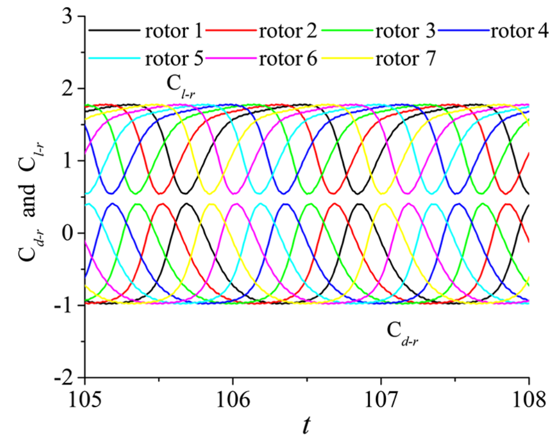

a) Drag and lift coefficients of rotor blades

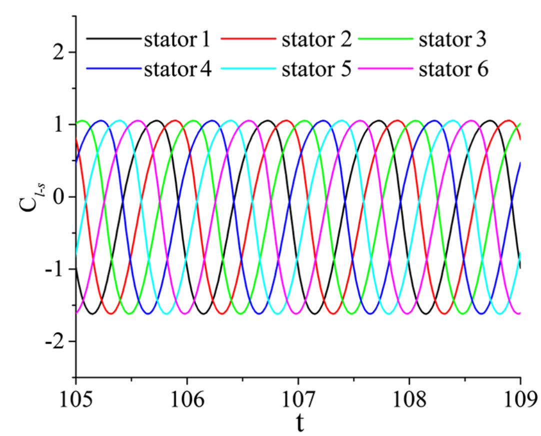

b) Lift coefficients of stator blades

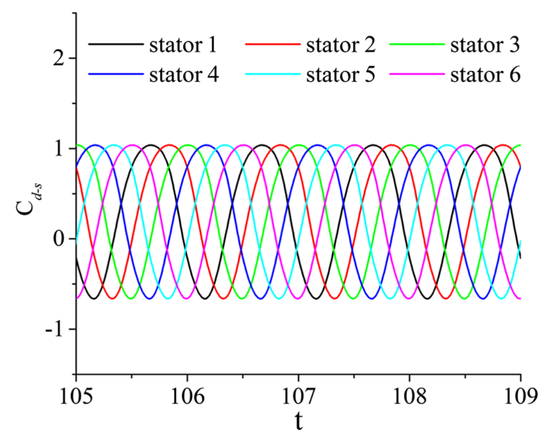

c) Drag coefficients of stator blades

Fig. 16 Drag and lift coefficients of blades versus time ($Re = 500$).

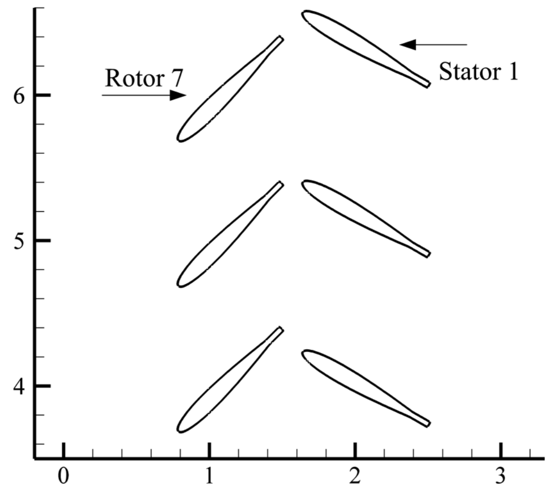

Fig. 17 Relative positions of rotor 7 and stator 1 at the instant of Fig. 15 (*Re* = 500).

The rotor rotation speed is used to define the lift and drag coefficients as

$$C_d = \frac{F_d}{\rho V^2 c/2} \tag{23}$$

$$C_l = \frac{F_l}{\rho V^2 c/2} \tag{24}$$

Figure 15 shows the vorticity field for $\delta/c = 0.13$ and $U = 0.5$ at $t = 107$ (in Fig. 16). The corresponding relative positions of rotor 7 and stator 1 are given in Fig. 17. Figure 16 shows the temporal variations of the drag and lift coefficients of the rotor and stator blades. A rotor blade sweeps past a stator blade for every $\Delta t = 7/6$, and a stator blade is influenced by the wake of a rotor blade for every $\Delta t = 1$.

The normalized coefficient of time-averaged total pressure rise is used to characterize the performance of a rotor/stator stage, defined as

$$\psi_n(\phi) = \frac{\Delta p_n^*}{(1/2)\rho V^2} = \frac{p_n^* - p_0^*}{(1/2)\rho V^2} \tag{25}$$

where p_n^* is the average total pressure at x_n ($n = 0, 1, 2$). The total pressure at the inlet is p_0^*, and x_1 corresponds to the middle of the rotor and stator. Also, x_2 is fixed at three chords after the trailing edge of the stage. The flow coefficient is denoted by $\phi = U/V$, and the total pressure rise of the stage is $p_2^* - p_0^*$.

Figure 18 shows the time-averaged total pressure coefficients ψ_1 and ψ_2 as functions of the flow coefficient. The differences in ψ_1 and ψ_2 indicate that the influence of the axial gap on the stage performance increases with decreasing flow coefficient. The maximum ψ_2 occurs at $\phi = 0.4$. The stage pressure rise decreases at $\phi = 0.3$ because the system approaches the stall margin. Figure 19 shows the temporal evolution of the total pressure rise coefficient ψ_{2t} for flow coefficients $\phi = 0.3$ and 0.4. The fluctuation of ψ_{2t} increases with decreasing blade spacing; this can be attributed to the generation of disordered flow between the rotor and stator. A decrease of the axial gap leads to enhanced average pressure rise along with increased fluctuations, as shown in Fig. 19.

Obviously, stage loading is determined by the lift on rotor blades. To determine the underlying mechanisms that dictate the effects of the axial blade gap on the stage performance, the drag and lift coefficients of the rotor blade are calculated for different values of δ for $\phi = 0.4$. Figure 20 indicates that the rotor blade lift increases when blade rows are brought closer together. The lift coefficient peaks are 0.62, 0.50, and 0.45 for $\delta/c = 0.03$, 0.08, and 0.13, respectively. The time-averaged lift coefficients are 0.382, 0.356, and 0.328, suggesting that the rotor blades can do more work. The

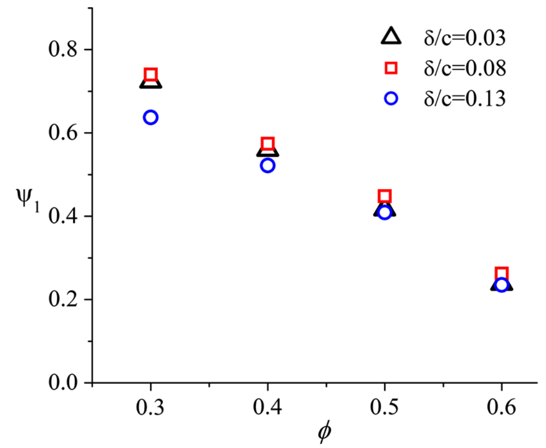

a) Time-averaged total pressure rise coefficients ψ_1

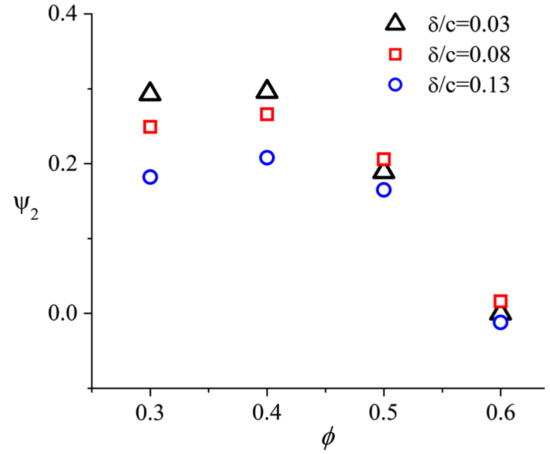

b) Time-averaged total pressure rise coefficients ψ_2

Fig. 18 Time-averaged total pressure rise coefficients ψ_1 and ψ_2 as functions of flow coefficient U/V = (*Re* = 500).

average total pressure rises are 0.294, 0.266, and 0.208, respectively, as shown in Fig. 18b. Meanwhile, the unsteadiness is enhanced by the reduction of the axial gap, as shown in Fig. 19. In this example, $\delta/c = 0.08$ is considered an optimal choice based on the tradeoff between the stage loading and flow unsteadiness.

Figures 21 and 22 show, respectively, the detailed vorticity and pressure fields around the trailing edge of the rotor blade for $\delta/c = 0.03$ and $\delta/c = 0.13$ at the instant of the maximum lift coefficient in Fig. 20. The interaction between adjacent blade rows becomes stronger when the axial gap decreases. The reduced axial gap between blade rows accelerates the fluid through the space between the rotor trailing edge and the stator leading edge when a rotor blade passes a stator blade. Figure 21 shows that the shedding vortices from the rotor trailing edge are visibly enhanced by the reduction of the axial gap. The reduced axial spacing also leads to the pressure difference shown in Fig. 22. The maximum vorticity around the trailing edge is 30.0 and 22.9 for $\delta/c = 0.03$ and 0.13, respectively, at the instant of rotor lift peak. As in the results reported by Li and Lu [24], the force generated on the blade is primarily determined by the vortical structure near the body. In the present study, the shedding vortical structures are enhanced through reduction of the axial gap between the rotor and stator. The enhanced vortex shedding from the trailing edge of the rotor blade suggests that a higher circulation is generated around the blade, indicating increased blade loading. The enhancement of the stage pressure rise with reduced blade spacing is thus corroborated.

This observation differs from the prevailing explanation of the mechanism of rotor/stator interaction in turbomachinery, in which the relevant mechanism is described as potential-flow interaction and viscous-wake interaction from upstream blade rows. In those models,

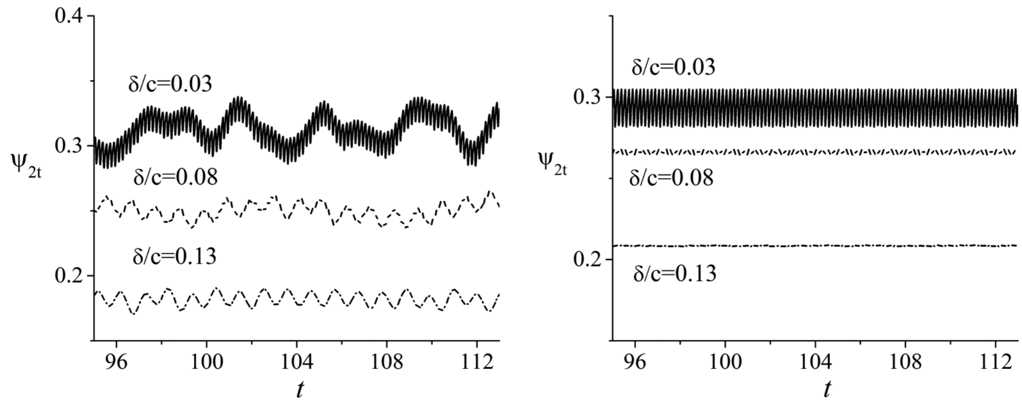

a) ϕ=0.3 b) ϕ=0.4

Fig. 19 Temporal evolution of total pressure rise coefficients ψ_{2t} of single stage for three different axial gaps between blade rows $\delta(Re = 500)$.

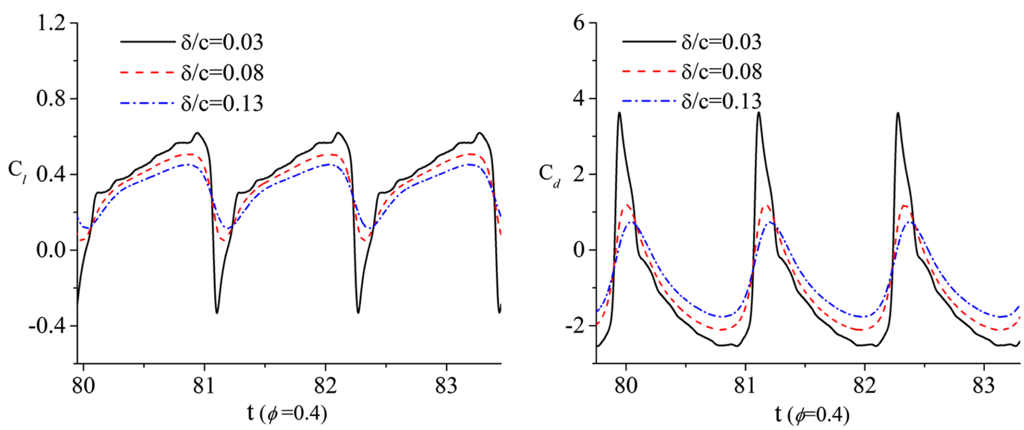

Fig. 20 Temporal evolution of drag and lift coefficients of rotor blades with different axial gaps between blade rows $\delta(\phi = 0.4, Re = 500)$.

the potential-flow interaction dominates the generation of the unsteady flowfield when the rotor/stator gap is reduced, with the viscous-wake interaction being the main cause of unsteadiness. The theory does not, however, explain the observations made in the present work. In fact, when the pressure field associated with the trailing edge of a rotor sweeps past the leading edge of a downstream stator, the strength of the potential interaction increases with decreasing rotor/stator gap. More important, vortex formation on both the trailing edge of the rotor and the leading edge of the stator is the primary result of such an interaction, and this requires an accurate description of both the potential flow and viscous effects. From this perspective, the generation of vortex lift due to rotor/stator interaction is similar to the high-lift formation of insects [13–21].

B. Rotor/Stator Interaction in Compressible Turbulent Flow

The previous example deals with incompressible laminar flows. Turbomachinery, however, usually involves compressible turbulent flow. We thus consider the following conservation equations for compressible flows:

$$\frac{\partial \rho}{\partial t} + \frac{\partial}{\partial x_j}(\rho u_j) = 0 \tag{26}$$

$$\frac{\partial \rho u_i}{\partial t} + \frac{\partial}{\partial x_j}(\rho u_j u_i) = -\frac{\partial p}{\partial x_i} + \frac{\partial \tau_{ij}}{\partial x_j} + \sum_{l=1}^{M} \boldsymbol{F}_k \tag{27}$$

$$\frac{\partial}{\partial t}\left[\rho\left(e + \frac{u_i u_i}{2}\right)\right] + \frac{\partial}{\partial x_j}\left[h + \frac{u_i u_i}{2}\right] = \frac{\partial}{\partial x_j}(u_i \hat{\tau}_{ij}) + \sum_{k=1}^{M}(\boldsymbol{u} \cdot \boldsymbol{F}_k) \tag{28}$$

where e is the internal energy, h is the enthalpy, $\hat{\tau}_{ij}$ is the viscous stress tensor, and $\boldsymbol{F}_k$ is the boundary forces. A k-ε model is employed in the present work to calculate the Reynolds stress tensors.

Although the large-eddy-simulation (LES) technique offers improved accuracy for complicated flows, especially separated flow, the computational time and memory demands of LES are high. Many studies [8,32,50,51] of rotor/stator interactions in turbomachinery have employed one-equation and two-equation models to achieve turbulence closure. Chima [50] compared the results with the Baldwin–Lomax and k-ω model for blade-to-blade flows in turbomachinery, and it was found that the k-ω model behaved well numerically and could reasonably simulate the effects of transition, freestream turbulence, and surface roughness. The k-ω model features properties similar to those of the k-ω model [52], and it can be used to predict the evolution of a given turbulent flow with no prior knowledge of the turbulence structure [53]. Considering the numerical behavior and computational requirements, the k-ω model is selected for the present work. The closure coefficients proposed by Wilcox [53] are used, as shown in Table 2. The same numerical scheme is used as in the simulations of laminar flow. The present method was successfully used by Du et al. [43] to predict the compressible turbulent flow of a modulated fan with pitching blades; that study showed that the present numerical method is reliable for solving unsteady flows at high Reynolds numbers. For the present study, we first validate the model against a flat-plate boundary layer at $Re = 2 \times 10^5$. The calculated velocity profile is shown in Fig. 23.

A compressor stage consisting of two rotor and three stator blades is investigated, as depicted in Fig. 24. The blade has the NACA2606 airfoil shape, and the chord is 0.1. Table 3 lists the geometric and flow parameters, where the Reynolds number is defined by Eq. (22). $Ma_r = |V|/c_0$ is the Mach numbers, and c_0 is the speed of sound. Four different axial gaps are studied in this section: $\delta/c = 0.05, 0.07, 0.12$, and 0.17. At the inlet, the total pressure, total temperature, and velocity angle are specified as the boundary conditions. At the exit,

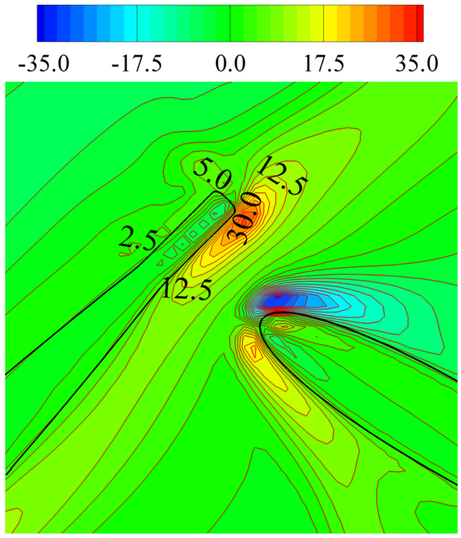

a) δ/c = 0.03

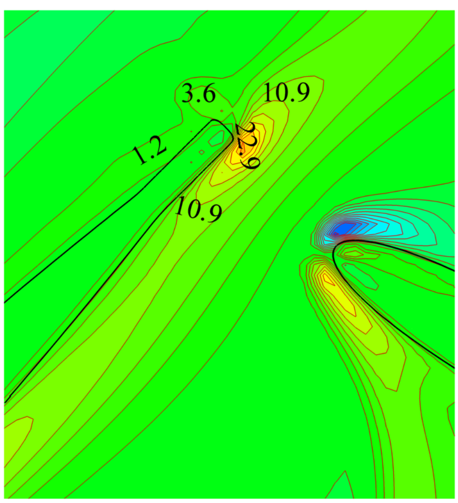

b) δ/c = 0.13

Fig. 21 Vorticity field around trailing edge of rotor blade at instant of lift peak for gaps of a) $\delta/c = 0.03$ and b) $\delta/c = 0.13$.

the static pressure is specified. Figure 25 shows the calculated static pressure rise when the axial gap is reduced from $\delta/c = 0.17$ to 0.05. Figure 26 shows the temporal evolution of the lift coefficient of the rotor blade for a flow coefficient of $\phi = 0.29$. At the peak of the rotor lift, the shedding vortices are enhanced by the rotor/stator interaction if the blade rows are brought closer, as shown in Fig. 27. The maximum vorticity near the trailing edge increases from 2.22×10^3 to 2.62×10^3, and the time averaged lift coefficient increases from 0.258 to 0.287 when the axial gap is reduced from $\delta/c = 0.12$ to 0.07. The peak rotor lift coefficient increases from 0.377 to 0.434. This phenomenon bears close similarity to its counterpart for an incompressible laminar flow.

Figures 28 and 29 show the velocity relative to the rotor blade at the instant of rotor lift peak in Fig. 26 for $\delta/c = 0.12$ and 0.17, respectively. The velocities around the trailing edge of the rotor blade increase when the gap between blade rows is reduced, especially in the circumferential direction. This phenomenon was not addressed in the study by Furber and Ffowcs Williams [12], in whose analytical model the gap between rotor and stator blades was zero. As discussed with a reference simulation of laminar flows, the enhancement of shedding vortices results from the acceleration of the fluid through the spacing between the rotor trailing edge and the stator leading edge. The peak lift increases with a reduced axial gap because the variation of circulation around the rotor blade is influenced by the

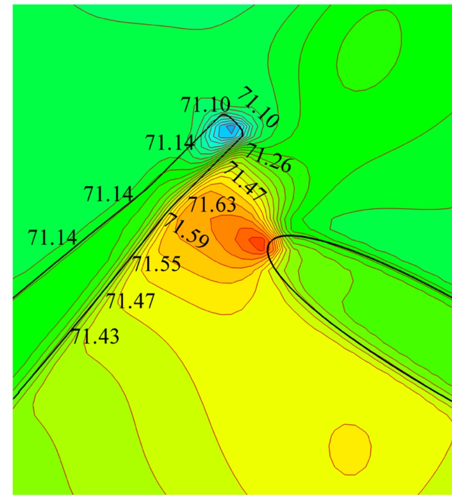

a) δ/c = 0.03

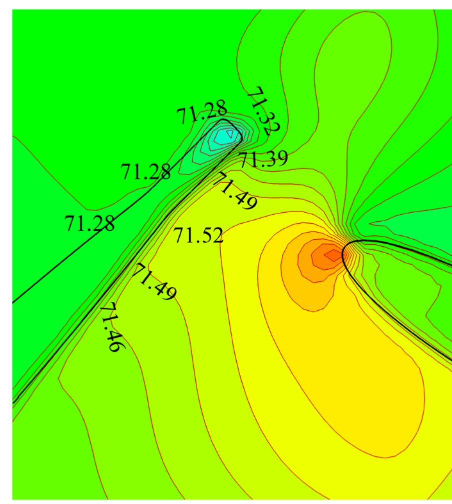

b) δ/c = 0.13

Fig. 22 Pressure field around rotor blade trailing edge at instant of lift peak for gaps of a) $\delta/c = 0.03$ and b) $\delta/c = 0.13$.

intensity of the shedding vortex. Although compressible turbulent flows are more complex, we obtain trends similar to those shown for laminar flows when the axial gap is reduced.

Table 2 Closure coefficients in the k-ω model

Parameter	Value
$C_{\varepsilon 1}$	1.44
$C_{\varepsilon 2}$	1.92
$C_{\varepsilon 1 \mu}$	0.09
σ_k	1.0
σ_ε	1.3

Table 3 Geometric parameters for the turbulent flow case

Parameter	Value
α_1	58 deg
α_2	−19 deg
Re	2×10^5
Ma_r	0.27
δ/c	0.05, 0.07, 0.12, 0.17

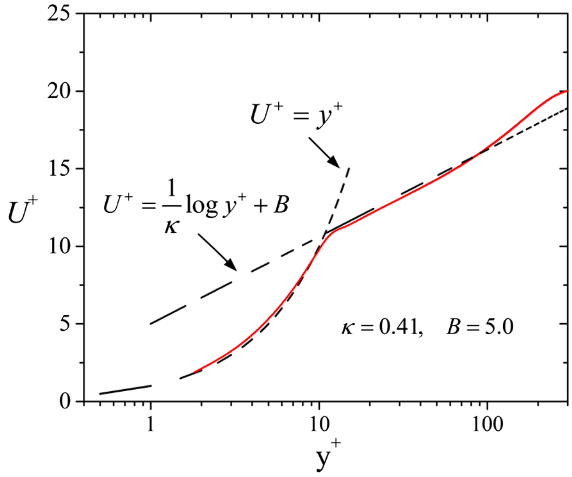

Fig. 23 Velocity profile for a turbulent boundary layer on a flat plate: $Re = 2 \times 10^5$.

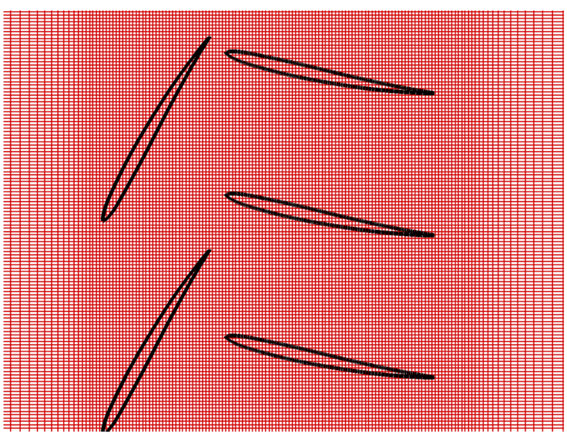

Fig. 24 Compressor stage consisting of two rotor blades and three stator blades, NACA 2606 blade: $\alpha_1 = 58$ deg, $\alpha_2 = -19$ deg, and $\delta = 0.07c$.

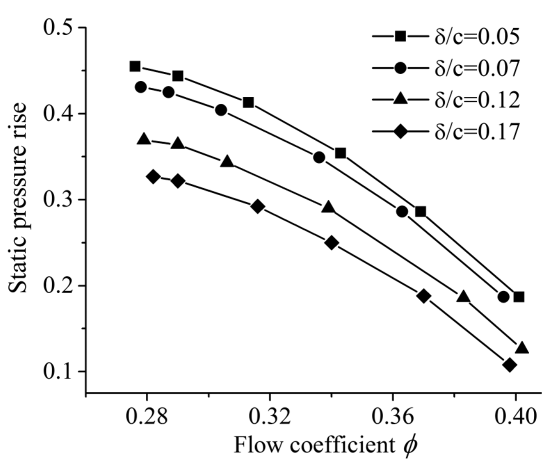

Fig. 25 Static pressure rise for different axial gaps ($U/V = 0.29$).

V. Conclusions

An effective numerical scheme based on the immersed boundary method is developed to study the flow associated with rotor/stator interaction on a quasi-three-dimensional coordinate system. Both laminar and turbulent cases are considered. Compared to conventional methods, the present approach has several advantages: a simple fixed Cartesian grid is used for the calculation, which makes it easy to generate the grid; and data transfer between the absolute and relative

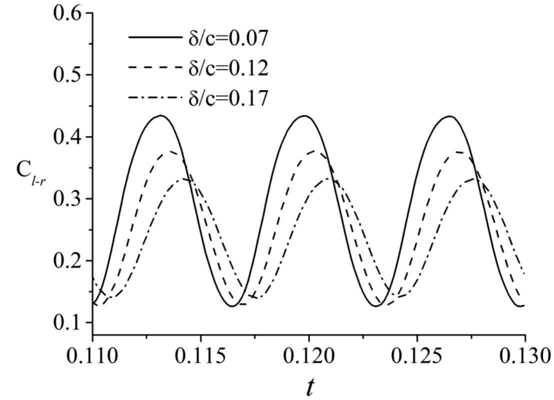

Fig. 26 Temporal evolution of rotor blade lift coefficient with different axial gaps between blade rows: $\phi = 0.29$.

frames of reference is avoided. The unsteady aerodynamic process can be simulated accurately, even when the axial gap between blade rows is very small.

By comparing with the inviscid model by Furber and Ffowcs Williams [12], the effect of viscosity and shedding vortices on the rotor/stator interaction can be included in the present work. The

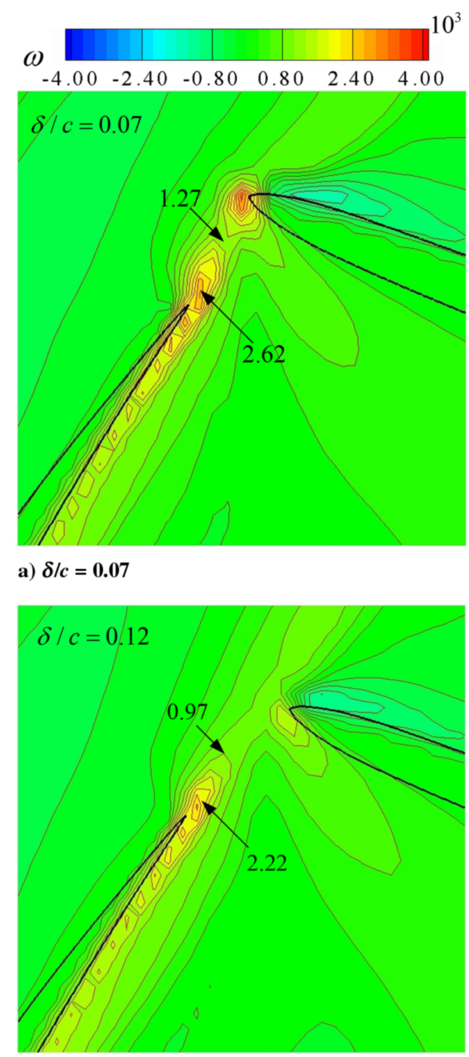

b) $\delta/c = 0.12$

Fig. 27 Vorticity field at peak of rotor blade lift coefficient, $\phi = 0.29$: $\delta/c = 0.07$ vs $\delta/c = 0.12$.

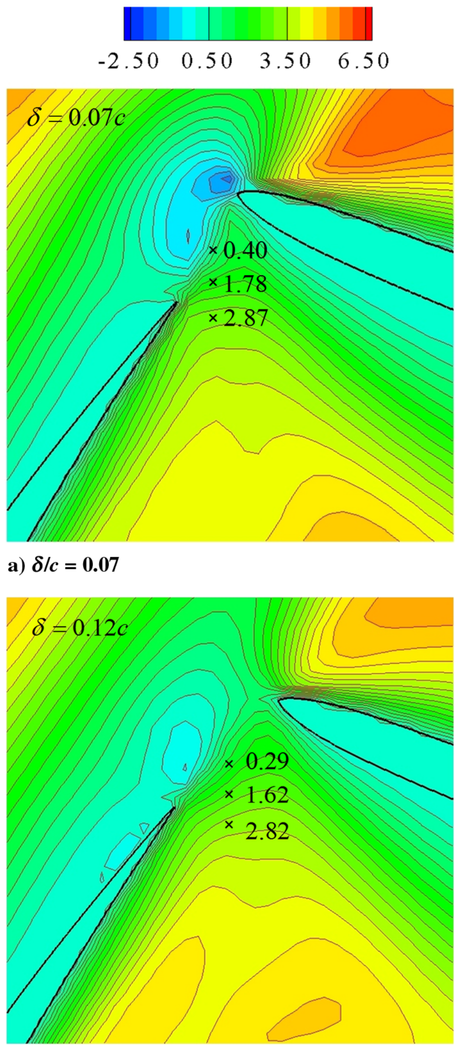

a) $\delta/c = 0.07$

b) $\delta/c = 0.12$

Fig. 28 Velocity field relative to rotor blade in axial direction at peak of rotor blade lift coefficient, $\phi = 0.29$: $\delta/c = 0.07$ vs $\delta/c = 0.12$.

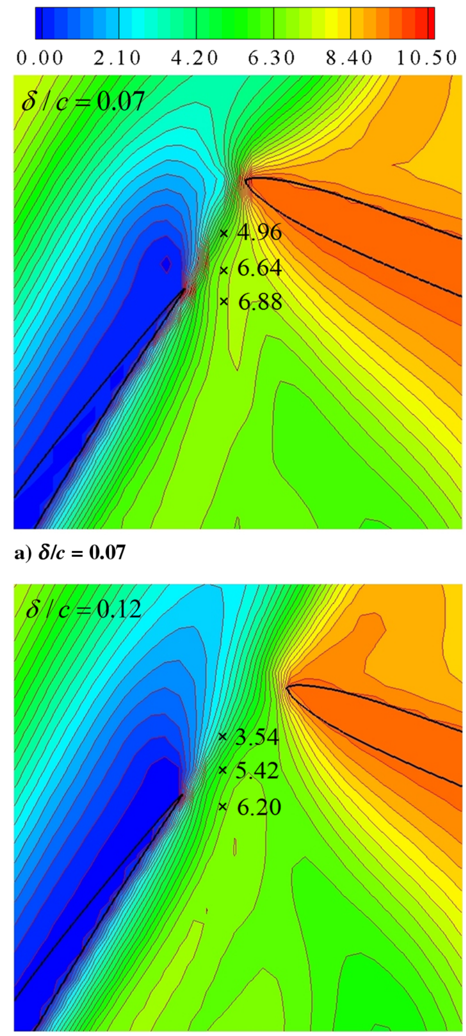

a) $\delta/c = 0.07$

b) $\delta/c = 0.12$

Fig. 29 Velocity field relative to rotor blade in circumferential direction at peak of rotor blade lift coefficient, $\phi = 0.29$: $\delta/c = 0.07$ vs $\delta/c = 0.12$.

numerical results show that the rotor blade average lift is enhanced with stronger shedding vortices at the trailing edge when the axial gap between blade rows is reduced. Thus, the stage loading can be increased, and this is beneficial to the thrust-to-weight ratio. In contrast to what is described by the Kutta–Joukowski theorem, and somewhat similar to the Weis–Fogh mechanism, this lift is due to the unsteady lift mechanism related to shedding vortices at the trailing edge of rotor blade. A high-lift peak is observed in each period of rotor/stator interaction. The fluid is accelerated by the rotor/stator interaction when the axial gap between blade rows is reduced. This leads to enhancement of the shedding vortex around the rotor blade. On the basis of Kelvin's theorem, the enhanced shedding vortices at the trailing edge of the rotor blade suggest that higher circulation is generated around the rotor blade, which in turn indicates that the blade force and loading increase. The proper axial gap must be chosen based on a study of unsteady flow passing though a rotor/stator stage because both the stage loading and the unsteadiness are heavily influenced by the interaction between adjacent blade rows, especially for a small axial gap. It should be noted that the vortical dynamics exhibit different characteristics in two-dimensional and 3-D flows. Three-dimensional vortex interactions involve much richer mechanisms, including possible room for further reducing the axial gap between rows. Further work on the 3-D model and related experiments will be required in order to obtain a better physical understanding of rotor/stator interactions.

Acknowledgments

The financial support of the National Natural Science Foundation of China (grant no. 51236001) and the 973 Program (grant no. 2012CB720200) are gratefully acknowledged.

References

[1] Dring, R. P., Blair, M. F., Joslyn, H. D., Power, G. D., and Verdon, J. M., "The Effects of Inlet Turbulence and Rotor/Stator Interactions on the Aerodynamics and Heat Transfer of a Large-Scale Rotating Turbine Model: IV – Aerodynamic Data Tabulation," NASA CR-4079, May 1986.

[2] Rao, K. V., and Delaney, R. A., "Investigation of Unsteady Flow Through a Transonic Turbine Stage: Part I-Analysis," AIAA Paper 1990-2408, 1990.

[3] Dunn, M. G., Bennett Delaney, R. A., and Rao, K. V., "Investigation of Unsteady Flow Through a Transonic Turbine Stage: Part II-Data/Prediction Comparison for Time-Averaged and Phase-Resolved Pressure Data," *Journal of Turbomachinery*, Vol. 31, No. 6, 1992, pp. 91–99. doi:10.1115/1.2928003

[4] Rangwalla, A. A., Madavan, N. K., and Johnson, P. D., "Application of an Unsteady Navier–Stokes Solver to Transonic Turbine Design," *Journal of Propulsion and Power*, Vol. 8, No. 5, 1992, pp. 1079–1086. doi:10.2514/3.23595

[5] Smith, L. H., Jr., "Casing Boundary Layers in Multistage Axial-Flow Compressors," *Flow Research in Blading*, edited by Dzung, L. S., Elsevier, Amsterdam, 1970, pp. 275–304.

[6] Gaetani, P., Persico, G., Dossena, V., and Osnaghi, C., "Investigation of the Flowfield in a High-pressure Turbine Stage for Two Stator-Rotor Axial Gaps—Part I: Three-Dimensional Time-Averaged Flowfield,"

Journal of Turbomachinery, Vol. 129, No. 3, 2007, pp. 572–579. doi:10.1115/1.2472383

[7] Funazaki, K., Yamada, K., Kikuchi, M., and Sato, H., "Experimental Studies on Aerodynamic Performance and Unsteady Flow Behaviors of a Single Turbine Stage with Variable Rotor-Stator Axial Gap: Comparisons with Time-Accurate Numerical Simulation," American Soc. of Mechanical Engineers Paper GT2007-27670, Fairfield, NJ, 2007.

[8] Yamada, K., Funazaki, K., Kikuchi, M., and Sato, H., "Influences of Axial Gap Between Blade Rows on Secondary Flows and Aerodynamic Performance in a Turbine Stage," American Soc. of Mechanical Engineers Paper GT2009–59855, Fairfield, NJ, 2009.

[9] Restemeier, M., Niewoehner, J., Jeschke, P., Guendogdu, Y., and Engel, K., "Experimental and Numerical Investigation of Blade Row Spacing Effects in 1.5 Stage Turbine Rig Under Off-Design Operating Conditions," *20th International Symposium on Air Breathing Engines*, AIAA, Reston, VA, 2011.

[10] Smith, L., "Wake Dispersion in Turbomachines," *Journal of Basic Engineering*, Vol. 88, No. 3, 1966, pp. 688–690. doi:10.1115/1.3645942

[11] Van Zante, D. E., Adamczyk, J. J., Strazisar, A. J., and Okiishi, T. H., "Wake Recovery Performance Benefit in a High-Speed Axial Flow Compressor," *Journal of Turbomachinery*, Vol. 124, No. 2, 2002, pp. 275–284. doi:10.1115/1.1445793

[12] Furber, S. B., and Ffowcs Williams, J. E., "Is the Weis–Fogh Principle Exploitable in Turbomachinery?" *Journal of Fluid Mechanics*, Vol. 94, No. 3, 1979, pp. 519–540. doi:10.1017/S0022112079001166

[13] Weis–Fogh, T., "Quick Estimates of Flight Fitness in Hovering Animals Including Novel Mechanism for Lift Production," *Journal of Experimental Biology*, Vol. 59, 1973, pp. 169–230.

[14] Lighthill, M. J., "On the Weis–Fogh Mechanism of Lift Generation," *Journal of Fluid Mechanics*, Vol. 60, No. 6, 1973, pp. 1–17. doi:10.1017/S0022112073000017

[15] Sun, M., and Lan, S.L., "A Computational Study of the Aerodynamic Forces and Power Requirements of Dragonfly Hovering," *Journal of Experimental Biology*, Vol. 207, 2004, pp. 1887–1901. doi:10.1242/jeb.00969

[16] Wang, J. K., and Sun, M., "A Computational Study of the Aerodynamic and Forewing-Hindwing Interaction of a Model Dragonfly in Forward Flight," *Journal of Experimental Biology*, Vol. 208, Pt. 19, 2005, pp. 3785–3804.

[17] Alexander, D. E., "Unusual Phase Relationships Between the Forewings and Hind Wings in Flying Dragonflies," *Journal of Experimental Biology*, Vol. 109, 1984, pp. 379–383.

[18] Ellington, C. P., "The Aerodynamics of Hovering Insect Flight. I-V," *Philosophical Transactions of the Royal Society of London, Series B: Biological Sciences*, Vol. 305, No. 1122, 1984, pp. 1–181. doi:10.1098/rstb.1984.0052

[19] Norberg, R. A., "Hovering Flight of the Dragonfly Aeschna Juncea L., Kinematics and Aerodynamics," *Swimming and Flying in Nature*, edited by Wu, T. Y., Brokaw, C. J., and Brennen, C., Vol. 2, 1975, Plenum Press, New York, pp. 763–781.

[20] Wang, Z.J., "Dissecting Insect Flight," *Annual Review of Fluid Mechanics*, Vol. 37, Jan. 2005, 183–210. doi:10.1146/annurev.fluid.36.050802.121940

[21] Wang, Z. J., and Russell, D., "Effect of Forewing and Hindwing Interactions on Aerodynamic Forces and Power in Hovering Dragonfly Flight," *Physical Review Letters*, Vol. 99, No. 14, 2007, pp. 14081.1–14081.4.

[22] Zhang, J., and Lu, X.-Y., "Aerodynamic Performance Due to Forewing and Hindwing Interaction in Gliding Dragonfly Hovering," *Physical Review E: Statistical, Nonlinear, and Soft Matter Physics*, Vol. 80, No. 6, 2009, Paper 017302. doi:10.1103/PhysRevE.80.017302

[23] Shyy, W., Aono, H., Chimakurthi, S. K., Trizila, P., Kang, C.-K., Cesnik, C. E. S., and Liu, H., "Recent Progress in Flapping Wing Aerodynamics and Aeroelasticity," *Progress in Aerospace Sciences*, Vol. 46, No. 7, 2010, pp. 284–327.

[24] Li, G-J., and Lu, X-Y., "Force and Power of Flapping Plates in a Fluid," *Journal of fluid Mechanics*, Vol. 712, Dec. 2012, pp. 598–613.

[25] Maxworthy, T., "Experiments on the Weis–Fogh Mechanism of Lift Generation by Insects in Hovering Flight. Part 1. Dynamics of the Fling," *Journal of Fluid Mechanics*, Vol. 93, No. 6, 1979, 47–63. doi:10.1017/S0022112079001774

[26] Spedding, G. R., and Maxworthy, T., "The Generation of Circulation and Lift in a Rigid Two-Dimensional Fling," *Journal of Fluid Mechanics*, Vol. 165, No. 6, 1986, 247–272. doi:10.1017/S0022112086003087

[27] Edwards, R. H., and Cheng, H. K., "The Separation Vortex in the Weis–Fogh Circulation-Generation Mechanism," *Journal of Fluid Mechanics*, Vol. 120, No. 6, 1982, pp. 463–473. doi:10.1017/S0022112082002857

[28] Rai, M. M., "Navier–Stokes Simulations of Rotor-Stator Interaction Using Patched and Overlaid Grids," AIAA Paper 1985-1519, 1985.

[29] Rai, M. M., "A Conservative Treatment of Zonal Boundaries for Euler Equation Calculations," *Journal of Computational Physics*, Vol. 62, No. 2, 1986, pp. 472–503. doi:10.1016/0021-9991(86)90141-5

[30] Giles, M., "Stator/Rotor Interaction in a Transonic Turbine," *Journal of Propulsion and Power*, Vol. 6, No. 5, 1990, pp. 621–627. doi:10.2514/3.23263

[31] Chima, R. V., "Explicit Multigrid Algorithm for Quasi-Three-Dimensional Viscous Flows in Turbomachinery," *Journal of Propulsion and Power*, Vol. 3, No. 5, 1987, pp. 397–405. doi:10.2514/3.23004

[32] Jorgenson, P. C. E., and Chima, R. V., "An Explicit Rung-Kutta Method for Unsteady Rotor/Stator Interaction," AIAA Paper 1988-0049, 1988.

[33] Hirt, C. W., and Nichols, B. D., "Volume of Fluid (VOF) Method for the Dynamics of Free Boundaries," *Journal of Computational Physics*, Vol. 39, No. 6, 1981, pp. 201–225. doi:10.1016/0021-9991(81)90145-5

[34] Osher, S., and Sethian, J. A., "Fronts Propagating with Curvature-Dependent Speed: Algorithms Based on Hamilton-Jacobi Formulations," *Journal of Computational Physics*, Vol. 79, No. 6, 1988, pp. 12–49. doi:10.1016/0021-9991(88)90002-2

[35] Eldredge, J. D., Leonard, A., and Colonius, T., "A General Deterministic Treatment of Derivatives in Particle Methods," *Journal of Computational Physics*, Vol. 180, No. 2, 2002, pp. 686–709. doi:10.1006/jcph.2002.7112

[36] Eldredge, J.D., "Numerical Simulation of the Fluid Dynamics of 2D of Rigid Body Motion with the Vortex Particle Method," *Journal of Computational Physics*, Vol. 221, No. 2, 2006, pp. 626–648. doi:10.1016/j.jcp.2006.06.038

[37] Cottet, G.-H., and Koumoutsakos, P., *Vortex Methods: Theory and Practice*, Cambridge Univ. Press, Cambridge, England, U.K., 2000, pp. 10–205.

[38] Peskin, C. S., "Numerical Analysis of Blood Flow in the Heart," *Journal of Computational Physics*, Vol. 25, No. 3, 1977, pp. 220–252. doi:10.1016/0021-9991(77)90100-0

[39] Goldstein, D., Handler, R., and Sirovich, L., "Modeling a No-Slip Flow Boundary with an External Force Field," *Journal of Computational Physics*, Vol. 105, No. 2, 1993, pp. 354–366. doi:10.1006/jcph.1993.1081

[40] Zhong, G, and Sun, X., "New Simulation Strategy for an Oscillating Cascade in Turbomachinery Using Immersed-Boundary Method," *Journal of Propulsion and Power*, Vol. 25, No. 2, 2009, pp. 312–321. doi:10.2514/1.35347

[41] Du, L., Jing, X., and Sun, X., "Modes of Vortex Formation and Transition to Three-Dimensionality in the Wake of a Freely Vibrating Cylinder," *Journal of Fluids and Structure*, Vol. 49, 2014, 554–573. doi:10.1016/j.jfluidstructs.2014.05.012

[42] Du, L., and Sun, X., "Suppression of Vortex-Induced Vibration Using the Rotary Oscillation of a Cylinder," *Physics of Fluids*, Vol. 27, No. 2, 2015, Paper 023603. doi:10.1063/1.4913353

[43] Du, L., Jing, X., Sun, X., and Song, W., "Aeroacoustic Model of a Modulation Fan with Pitching Blades as a Sound Generator," *Journal of the Acoustical Society of America*, Vol. 136, No. 4, 2014, pp. 1542–1551. doi:10.1121/1.4893904

[44] Park, J., and Garcés, M., "The Rotary Subwoofer: A Controllable Infrasound Source," *Journal of the Acoustical Society of America*, Vol. 125, No. 4, 2009, pp. 2006–2012. doi:10.1121/1.3082115

[45] Ming-Chih, L., and Peskin, C. S., "An Immersed Boundary Method with Formal Second-Order Accuracy and Reduced Numerical Viscosity," *Journal of Computational Physics*, Vol. 160, No. 2, 2000, pp. 705–719. doi:10.1006/jcph.2000.6483

[46] Armfield, S., and Street, R., "The Fractional-Step Method for the Navier–Stokes Equations on Staggered Grids: The Accuracy of Three Variations," *Journal of Computational Physics*, Vol. 153, No. 2, 1999, pp. 660–665. doi:10.1006/jcph.1999.6275

[47] Lima E Silva, A. L. F., Silveira-Neto, A., and Damasceno, J. J. R., "Numerical Simulation of Two-Dimensional Flows over a Circular Cylinder Using the Immersed Boundary Method," *Journal of Computational Physics*, Vol. 189, No. 2, 2003, pp. 351–370. doi:10.1016/S0021-9991(03)00214-6

[48] Wieselsberger, C., "New Data on the Laws of Fluid Resistance," NACA TN-84, 1922.

[49] Miller, L. A., and Peskin, C. S., "When Vortices Stick: An Aerodynamic Transition in Tiny Insect Flight," *Journal of Experiment Biology*, Vol. 207, No. 17, 2004, pp. 3073–3088. doi:10.1242/jeb.01138

[50] Chima, R. V., "Application of the K-Omega Turbulence Model to Quasi-Three-Dimensional Turbomachinery Flows," *Journal of Propulsion and Power*, Vol. 12, No. 6, 1996, pp. 1176–1179. doi:10.2514/3.24159

[51] Rai, M. M., "Unsteady Three-Dimensional Navier–Stokes Simulations of Turbine Rotor-Stator Interaction," AIAA Paper 1987–2058, 1987.

[52] Wilcox, D. C., "Reassessment of the Scale Determining Equation for Advanced Turbulence Models," *AIAA Journal*, Vol. 26, No. 11, 1988, pp. 1299–1310. doi:10.2514/3.10041

[53] Wilcox, D. C., *Turbulence Modeling for CFD*, DCW Industries, Inc., La Canada, CA, 1993, pp. 83–89.

F. Liu
Associate Editor